Results in Physics 23 (2021) 103939

Contents lists available at ScienceDirect

Results in Physics

journal homepage: www.elsevier.com/locate/rinp

Optical-electronic performance and mechanism investigation of dihydroindolocarbazole-based organic dyes for DSSCs

Qian Liu [a,b,*], Shihan Zhao [a], Yanhua Zhai [b], Ming Xu [a], Miao Li [a], Xianbin Zhang [a,*]

[a] Department of Applied Physics, Xi'an University of Technology, Xi'an 710054, China
[b] Department of Physics, Kennesaw State University, Marietta, GA 30060, USA

ARTICLE INFO

Keywords:
Dye-sensitized solar cells
Organic dyes
Density functional theory
Charge transfer

ABSTRACT

In recent years, organic dye molecules as photosensitizers have played a significant role in the field of dye-sensitized solar cells. In this context, two primary dihydroindolocarbazole-based organic dyes (sk201 and sk202), which were synthesized recently by Song et al., and three further designed dyes (DMZ1-3) were theoretically investigated based on density functional theory and time-dependent density functional theory. Molecular geometries, absorption spectra, charge transfer, molecular electrostatic potential and nonlinear optical properties were quantificationally studied and visually presented to reveal the relationships between the molecular structures and performances of dyes. The effects of joining the isolated dyes and TiO_2 on the molecular absorption spectra and energy levels were analyzed. Moreover, several parameters, such as efficiency of light-harvesting, driving forces of electron regeneration and injection, excited-state lifetime and vertical dipole moment, were calculated to give the multi-angle demonstrations of the photovoltaic performances for these dyes.

Introduction

With the progress of human society and industry development, the world's demand for energy is increasing day by day, which has caused global environmental problems to be more and more prominent [1,2]. Nowadays, multiple renewable energy sources (including hydropower, wind power, and solar power and so on) are being investigated to overcome the issues caused by conventional fossil fuels. Solar power based on photovoltaic cells is regarded as the cleanest, safest and most abundant source, which is the most promising alternative to achieve the above goal [3]. As one of solar technologies, dye-sensitized solar cells (DSSCs) are now regarded as an economical and reliable alternative to substitute for fossil fuels due to the relatively high performance, ease of fabrication and low manufacturing cost [4–7].

Generally, a DSSC device has four components: semiconductor oxide nanoporous membrane, dye sensitizer, redox electrolyte and the counter electrode. Among them, dye sensitizer is undoubtedly the core component responsible for capturing photons and then injecting the excited electrons into the semiconductor (TiO_2) nanocrystalline film. In the past two decades, every breakthrough in DSSCs is closely related to the progress of dye sensitizers, and plenty of high-efficiency dyes (mainly including zinc porphyrin dyes, Ru complex dyes and push-pull organic dyes) were investigated for continuously improving the total photoelectric conversion efficiencies (PCEs) of DSSCs from 10% to 14% [8–12]. In recent years, organic dye sensitizers, usually characterized by electron donor-conjugated π bridge-electron acceptor (D-π-A) configuration, have attracted great attention in the field of DSSCs for their ease to synthesize, flexible molecular design, higher molar extinction coefficients and environmentally friendly character [13–20].

Many novel organic dyes, especially the metal-free organic dyes, were reported in the context of DSSCs. Sun et al. reported four D-π-A type organic dyes (PCT1-4), and concluded that the cyclopentadipyrrole unit used for the π-bridges would improve the performances of DSSCs [21]. Lu et al. also discussed the impacts of π-bridges on the properties of dyes and found that dyes' performances may be deteriorated by extending π-conjugated bridges caused by the increased recombination of charges [22]. Galappaththi et al. designed a cyanidin-based dye molecule (P01-1) and investigated their absorption spectra and electronic structures to reveal its performances for DSSCs [23]. In terms of the experiment, Liu et al. synthesized a series of indacenodithiophene (IDT)-based organic dyes with different electron acceptors, which achieved a high open-circuit voltage (>1.1 V) and high PCEs of 11.2% by manipulating electron affinity [24]. Ren et al. reported a new blue dye (R6) designed for DSSC, which conducted the highest PCE (12.6%)

* Corresponding authors at: Department of Applied Physics, Xi'an University of Technology, Xi'an 710054, China (Q. Liu).
E-mail addresses: liuqian@xaut.edu.cn (Q. Liu), zhangxianbin@xaut.edu.cn (X. Zhang).

https://doi.org/10.1016/j.rinp.2021.103939
Received 27 May 2020; Received in revised form 1 November 2020; Accepted 1 February 2021
Available online 16 February 2021

among the blue pigments [25]. Cheng et al. synthesized a series of dyes (XC1-XC5), and investigated the co-sensitization of these dyes and another porphyrin-based dye XW28, in which the highest PCE of 10.50% was achieved for the co-sensitization of XC5 and XW28 [26]. Zeng et al. designed and synthesized two doubly strapped porphyrin sensitizers (XW40 and XW42) with PCE of 9.3% (for XW40) and 8.2% (for XW41), which were increased to 10.6% (for XW40) and 10.2% (for XW41) in the cases of co-adsorption with CDCA and co-sensitization with Z1 [27]. Desta et al. investigated a series of D-A-π-A type sensitizers (MD4-MD7) featuring the auxiliary acceptor (thieno[3,4-b]pyrazine or benzo[3,4-b] pyrazine), in which MD7 showed the best efficiency of 9.03% with help of the co-adsorbent (1 mM CDCA) [28].

In this work, two primary dihydroindolocarbazole-based organic dyes (sk201 and sk202) synthesized lately by Song et al. [29] and three further designed dyes (DMZ1, DMZ2 and DMZ3) were theoretically investigated as the photosensitizers for DSSCs. Based on DFT [30,31] and TD-DFT [32], the optimized molecular structures, energy levels and gaps, and absorption characteristics of light were calculated and compared with experimental results [29]. The changes in dyes' properties before and after absorbing on TiO_2 were emphatically studied. Besides, the frontier molecular orbitals (FMOs) and charge difference density (CDD) were employed to visually show the intramolecular charge transfer (ICT) for the dyes. For quantificationally demonstrating and comparing the photovoltaic performances of the dyes, the oxidation potential, the driving forces of electron regeneration and injection, the lifetime of dye molecule in the excited state, the vertical dipole moment, and the light-harvesting efficiency (LHE) were calculated to give the multi-angle demonstrations of the photovoltaic performances for these dyes.

Computational method

Density functional theory (DFT) with B3LYP functional [33,34] was used to optimize the molecular geometries of the investigated dyes in the ground state (before and after absorbing on TiO_2). 6-31G (d) and LANL2DZ [35] were chosen as the basis sets for the nonmetallic atoms and Ti atoms, respectively. For the isolated dyes (before absorbing on TiO_2), the optimizations of dye molecules were carried out in both gas and dichloromethane (DCM) solvent with conductor-like polarizable continuum model [36]. Herein the DCM solvent was selected to be compared with the experimental results [29]. In the dye/TiO_2 complexes (after dyes absorbing on TiO_2), which are the actual forms of dyes in DSSCs, the optimized calculations were only performed in DCM solvent. Here, $(TiO_2)_9$ nanocluster and bidentate bridging adsorption model [37], which have been widely used before [38–42], were employed to explore the adsorption effects between dyes and TiO_2 on the properties of dyes/TiO_2 complexes. Furthermore, time-dependent DFT (TD-DFT) was used to study the properties of dye molecules in the excited state at CAM-B3LYP [43]/6-311G(d, p) level. All calculations based on DFT and TD-DFT were done with the Gaussian 16 package [44]. The wave-function analyses were carried out with Multiwfn 3.39 [45].

Results and discussion

Molecular structures

The properties of dyes used for photosensitizers, such as the absorption spectrum and ICT, effectively influence the photoelectric performances of DSSCs that are closely related to the molecular structures. Fig. 1 shows the molecular structures of the primary dye molecules (sk201 and sk202), of which the different moieties were highlighted in different colors. Their optimized geometries were given in Fig. S1. Obviously, sk201 and sk202 share the same electron donor (5,11-dihydroindolo[3,2-b]carbazole derivative, DDC) and the same electron acceptor (4-(benzo[c][1,2,5]thiadiazol-4-ylethynyl)benzoic acid, BTZ) [29]. The only difference is that the donor and acceptor of sk201 are directly connected through a single bond, whereas a thiophene unit is inserted in the same position of sk202. Some important dihedral angles of the optimized molecular geometries were calculated and shown in Fig. 1. For sk201, the dihedral angles between the donor and acceptor are 34° in gas and 36° in DCM solvent. For sk202, a twisted structure (28° in gas and 24° in DCM solvent) exists between the donor and thiophene unit, and another smaller twist (7° in gas and 0° in DCM solvent) can be found between the thiophene unit and the acceptor. Because of the previous works [46], these proper twisted structures help

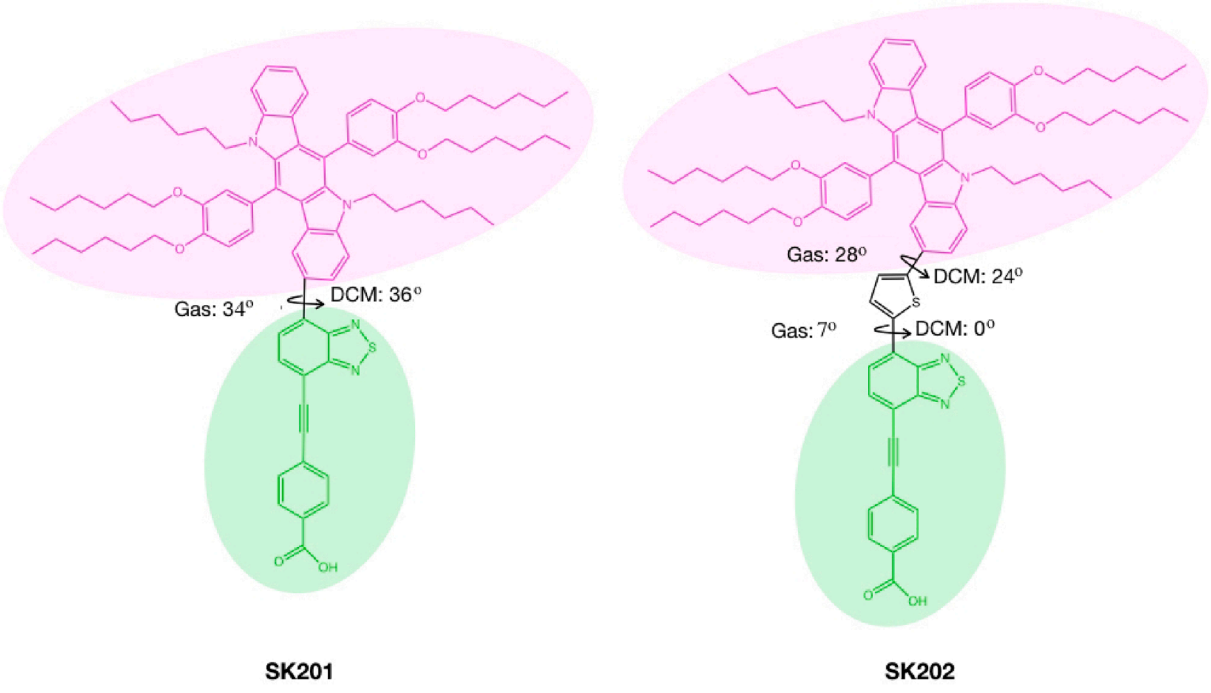

Fig. 1. Molecular structures of dyes (sk201 and sk202).

inhibit dye molecules' aggregation on TiO_2 films. Besides, due to thiophene's presence, sk202 exhibits a relatively better overall planarity and a higher degree of conjugation than sk201, which will promote charge delocalization and ICT of sk202. The superiorities of sk202 over sk201 in charge delocalization and ICT will be further demonstrated in the following sections.

Excited-state characteristics and absorption spectra

A broad and strong absorption of visible light is an essential requirement for the dyes used for DSSCs. Fig. 2 shows the computed absorption spectra curve of the investigated dyes. The involved excitation energy (E_g), wavelengths corresponding to the maximum absorption (λ_m), molecular orbital (MO) transitions and oscillator strengths (f) were listed in Table 1. From Fig. 2, both sk201 and sk202 exhibit the typical characteristic of dual absorption peaks. One peak located in the near-ultraviolet region, which arises from the π-π* transitions of the whole conjugation backbone [47], is referred to as the secondary absorption peak herein. The other located in the visible region is the main absorption peak related to the ICT process between electron donor and electron acceptor [47]. Table 1 shows that the wavelengths of the main absorption peaks in the gas are 449 nm for sk201 and 499 nm for sk202. For the case in the DCM solvent, the maximum absorption wavelengths of sk201 and sk202 are 450 nm and 509 nm, respectively, close to the experimental results (sk201: 492 nm, sk202: 527 nm) [29]. Table 1 further explains the generation of the two absorption peaks for the dyes. All prominent absorption peaks are caused by the electron transition from the highest occupied molecular orbital (HOMO) to the lowest unoccupied molecular orbital (LUMO). The secondary absorption peaks are mainly generated by the change of HOMO (H) → LUMO (L) + 1, except for the case of sk202 in DCM solvent, which is related to the transition of H → L + 3. Moreover, to show the effects of connecting to TiO_2 on the dyes' spectra, the absorption curves of sk201/TiO_2 and sk202/TiO_2 were plotted in Fig. 2(b), which are also in good agreement with the experimental results [29]. It can be clearly seen from Fig. 2 and Table 1 that sk201/TiO_2 and sk202/TiO_2 have higher molar absorption coefficients than their isolated counterparts (sk201 and sk202), with only slight blue-shifts (sk201: 4 nm, sk202: 6 nm) in the maximum absorption wavelengths. By comparison, sk202 exhibits overwhelming advantages in the absorption intensity, maximum absorption wavelength and width of central absorption peak over sk201, which are related to its higher conjugation degree and better overall planarity of sk202 caused by the introduction of a thiophene unit.

Table 1
Calculated excitation energy (E_g/eV), maximum absorption wavelength (λ_m/nm), molecular orbital contributions and oscillator strengths (f) of dyes in different conditions.

Dyes	States	λ_m/E_g	MO Contributions	f
sk201 (Gas)	S1	449/2.7616	(0.56097) H → L	0.8843
	S2	354/3.4986	(0.51041) H-1 → L	0.0639
	S3	350/3.5385	(0.58624) H → L + 2	0.2426
	S4	332/3.7328	(0.40700) H-2 → L	0.0095
	S5	307/4.0418	(0.42467) H → L + 1	0.8791
	S6	299/4.1348	(0.61911) H-1 → L + 2	0.3820
sk201 (DCM)	S1	450/2.7558	(0.54777) H → L	1.0348
	S2	354/3.4982	(0.60451) H → L + 2	0.3251
	S3	352/3.5256	(0.43459) H-1 → L	0.0578
	S4	329/3.7672	(0.43964) H-1 → L	0.0071
	S5	308/4.0261	(0.39870) H → L + 1	0.9012
	S6	304/4.0834	(0.62433) H-1 → L + 2	0.6270
sk201/TiO_2 (DCM)	S1	446/2.7811	(0.42590) H → L	1.2131
	S2	351/3.5278	(0.30762) H → L	0.3304
	S3	347/3.5750	(0.17411) H-1 → L	0.1809
	S4	329/3.7710	(0.31111) H-1 → L	0.1090
	S5	322/3.8471	(0.30989) H → L	0.4068
	S6	313/3.9614	(0.66263) H → L + 1	0.0007
sk202 (Gas)	S1	499/2.4833	(0.53111) H → L	1.3559
	S2	369/3.3645	(0.41804) H → L	0.0247
	S3	352/3.5179	(0.62313) H → L + 2	0.1149
	S4	329/3.7681	(0.45785) H-2 → L	0.0331
	S5	320/3.8753	(0.34703) H → L + 1	1.1959
	S6	309/4.0186	(0.38434) H-3 → L	0.0269
sk202 (DCM)	S1	509/2.4354	(0.53280) H → L	1.5202
	S2	366/3.3887	(0.39386) H → L	0.0132
	S3	358/3.4621	(0.62537) H → L + 2	0.1544
	S4	324/3.8308	(0.32439) H → L + 3	0.9687
	S5	322/3.8514	(0.35844) H-2 → L	0.3630
	S6	308/4.0238	(0.39408) H-2 → L	0.0237
sk202/TiO_2 (DCM)	S1	503/2.4656	(0.51704) H → L	1.7156
	S2	363/3.4125	(0.37722) H → L	0.0389
	S3	350/3.5406	(0.21090) H-1 → L + 34	0.1564
	S4	334/3.7084	(0.25490) H → L + 6	0.8812
	S5	321/3.8565	(0.33821) H-1 → L	0.2621
	S6	321/3.8627	(0.64150) H → L	0.0001

Energy levels and gaps

The elected energy levels (HOMOs and LUMOs) and their gaps in the investigated dyes were numerically shown in Fig. 3. For a qualified dye

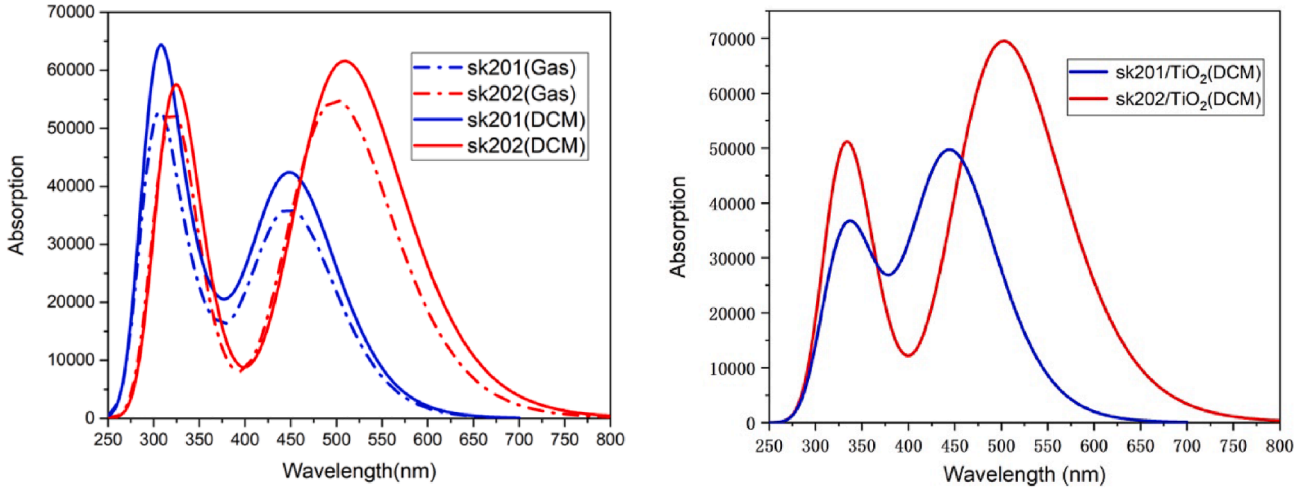

Fig. 2. The simulated curve of the absorption spectra of dyes in different conditions.

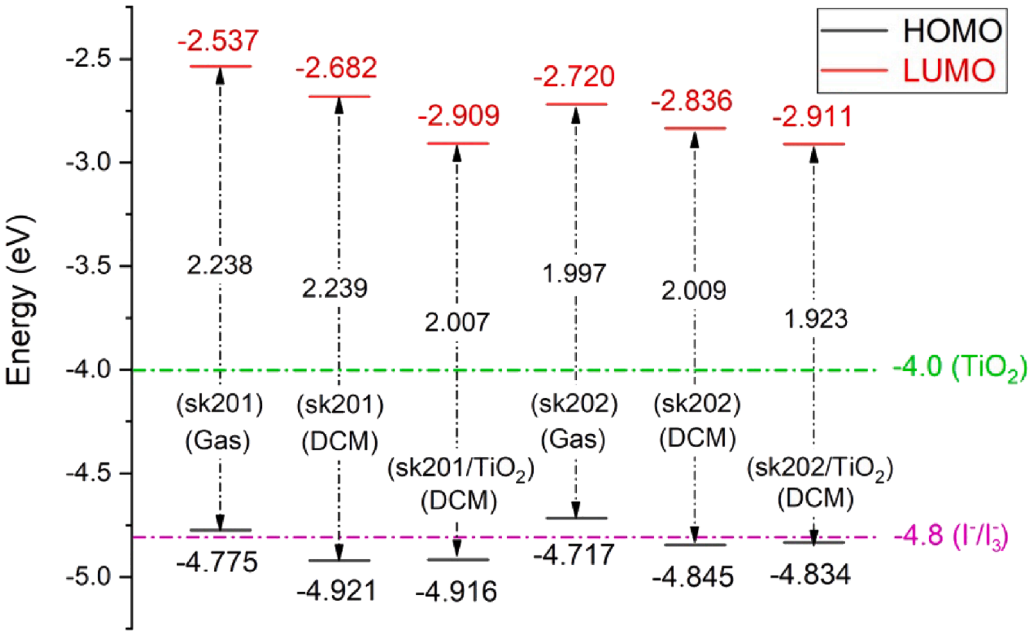

Fig. 3. Selected energy levels of sk201 and sk202 (before and after absorbing on TiO_2).

photosensitizer, the gap between HOMO and LUMO should cover the conduction band (CB) edge of TiO_2 (E_{CB} = 4.0 eV) and the redox potential (E_{redox}) of I^-/I_3^- (−4.6 eV in vacuum and −4.8 eV in solvent) for the effective electron injection and reduction of oxidized dyes [48,49]. As shown in Fig. 3, both isolated dyes and their dye/TiO_2 complexes (in solvent) match the above conditions required for HOMOs and LUMOs. Besides, Fig. 3 shows no noteworthy difference in the HOMO energy between the isolated dyes and the dye/TiO_2 complexes in the case of solvent. Still in the DCM solvent, the LUMOs of the two dyes decrease after absorbing on TiO_2 due to the strong coupling between the LUMOs and TiO_2, which is beneficial to injecting electrons into TiO_2. Based on the above comparison, it can be found that the dye/TiO_2 complex (sk201/TiO_2 or sk202/TiO_2) has a narrower gap between HOMO and LUMO than its corresponding isolated counterpart (sk201 or sk202). Meanwhile, sk202 shows narrower gaps than sk201 in DCM solvent, namely, 2.009 eV (sk202) < 2.239 eV (sk201), 1.923 eV (sk202/TiO_2) < 2.007 eV (sk201/TiO_2). It is known that a narrower gap between HOMO and LUMO will promote electron excitation with visible light and then improve light harvesting efficiency. Hence, sk202 will show a better light-harvesting efficiency than sk201, which accords with analysis in previous sections and is also in good agreement with experimental results.

Electronic structures and charges transfer characteristics

The electron cloud distributions of frontier molecular orbitals (FMOs) are the intuitive exhibitions of charge separation and ICT for dye molecules. Considering the transitions paths, which contribute to the dual absorption peaks, the electron cloud distributions of FMOs (H, L, L + 1, L + 2, L + 3) were calculated in DCM solvent and visually presented in Fig. 4. For the HOMOs of sk201 and sk202 in the ground state, the electron clouds mainly distribute on DDC and thiophene unit (only for sk202), with a small part spread to benzo[*c*][1,2,5]thiadiazole. For the LUMOs of the two dyes, the electron densities are almost completely transferred to the BTZ unit, and only a small part of electron densities remain in the donor. The transition of H → L results in a very efficient ICT process that corresponds to the dyes' main absorption peak. Besides, for the orbitals of L + 1 and L + 2, electron clouds are completely gathered in BTZ and DDC, respectively, for both dyes. For the L + 3 orbitals, electron clouds are mainly distributed on the BTZ and thiophene unit (only for sk202), with a small part spread to DDC for both dyes. The transitions of H → L + 1 and H → L + 3 are also ICT states, which generate the secondary absorption peak for sk201 and sk202, respectively.

For investigating the ICT properties of dyes after absorbing on TiO_2, the charge difference densities (CDD) of six excited states (S1-S6) were calculated for sk201/TiO_2 and sk202/TiO_2 in DCM solvent and visually shown in Fig. 5, in which the red and the green represent the densities of electrons and holes, respectively. For reducing the charge recombination between the injected electrons and the oxidized dyes, the holes should be confined to the donor of the dye molecule; that is, it will be away from the TiO_2. From Fig. 5, the complete charge transfer occurs in S5 and S6 for sk201/TiO_2, and S4 and S6 for sk202/TiO_2. Besides, the excited states (S1, S2, S3) of sk201/TiO_2 and sk202/TiO_2 can be attributed to the locally excited states, of which the electrons and holes partially overlap each other. By comparing with sk201, it is found that the introduction of a thiophene unit increases the hole distribution sites for sk202, which accelerates the separation of the intramolecular charge to a certain extent.

Besides, the charge transfer rate (w), which describe the intramolecular charge transfer in the dye molecules, can be calculated based on Marcus-Hush equation [60–63]:

$$w = \frac{V^2}{\hbar}\left(\frac{\pi}{\lambda_{total} kT}\right) exp\left(\frac{\lambda_{total}}{4kT}\right) \quad (1)$$

where V is the coupling matrix element decided by the energy of HOMO (E_{HOMO}) and HOMO − 1 ($E_{HOMO\text{-}1}$), kT is the thermal energy at absolute temperature T; λ_{total} is the reorganization energy, which has two parts: hole reorganization energy (λ_h) and electron reorganization energy (λ_e). V, λ_h and λ_e have the expressions, respectively [50–52].

$$V = \frac{1}{2}(E_{HOMO} - E_{HOMO-1}) \quad (2)$$

$$\lambda_h = (E_0^+ - E_+) + (E_+^0 - E_0) \quad (3)$$

$$\lambda_e = (E_0^- - E_-) + (E_-^0 - E_0) \quad (4)$$

where E_+, E_- and E_0 are the energy of cationic, anionic and neutral ground-state dye molecule, respectively. E_+^0 (E_-^0) and E_0^+ (E_0^-) are the

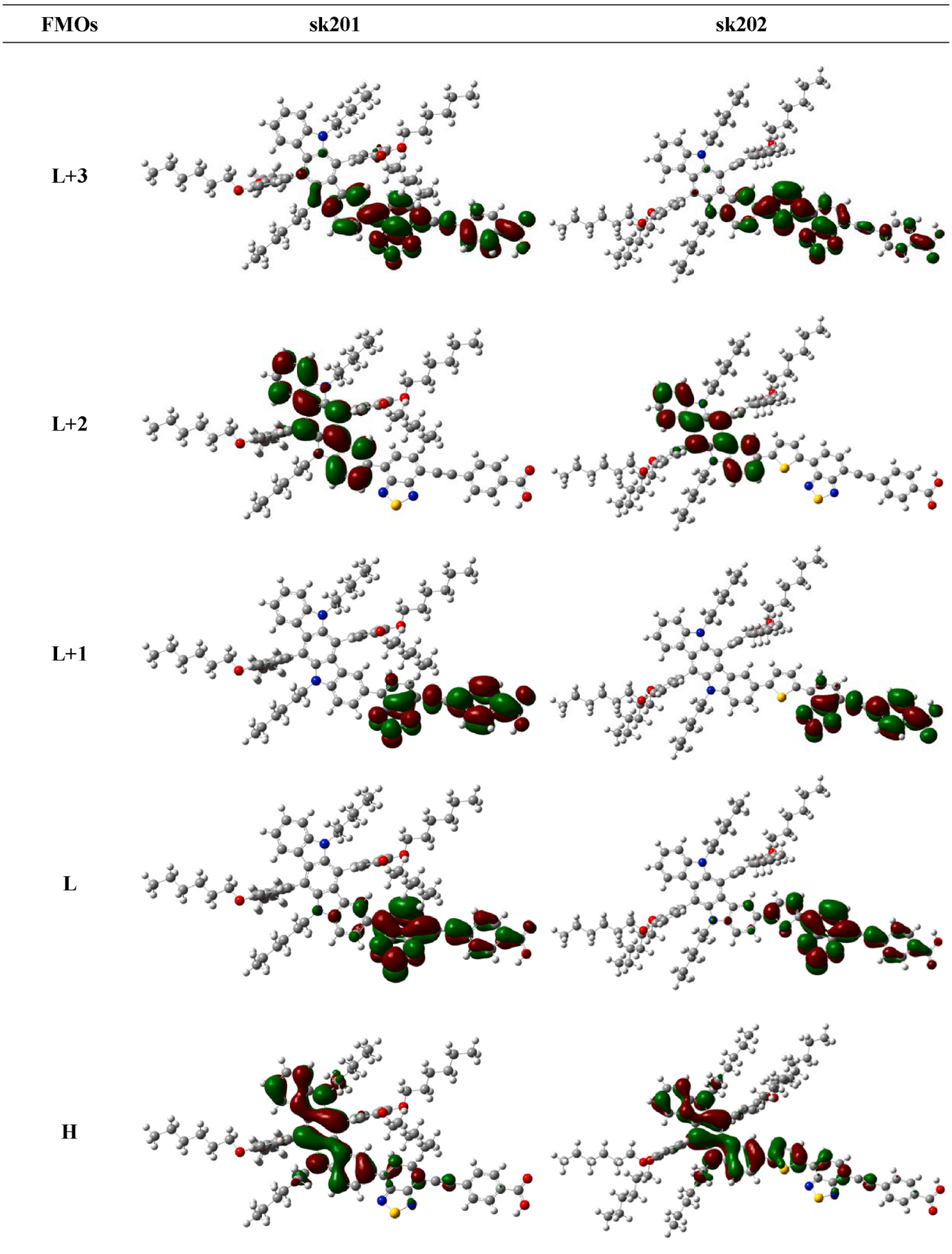

Fig. 4. Selected frontier molecular orbitals (FMOs) of sk201 and sk202 in DCM solvent.

energy of neutral dye molecule based on cationic (anionic) state and energy of anionic (anionic) dye molecule based on neutral state. From Eq. (1), a smaller λ_{total} will lead to a bigger w, namely, a better ICT process [53]. The values of λ_h, λ_e and λ_{total} were listed in Table 2. The λ_{total} of the sk202 and sk201 are 0.315 and 0.371, respectively, which indicates sk202 has a better charge transfer performances than sk201. In other words, sk202 is more conducive to produce a bigger photocurrent to improve the PCE. This also demonstrates that the introduction of thiophene can promote ICT.

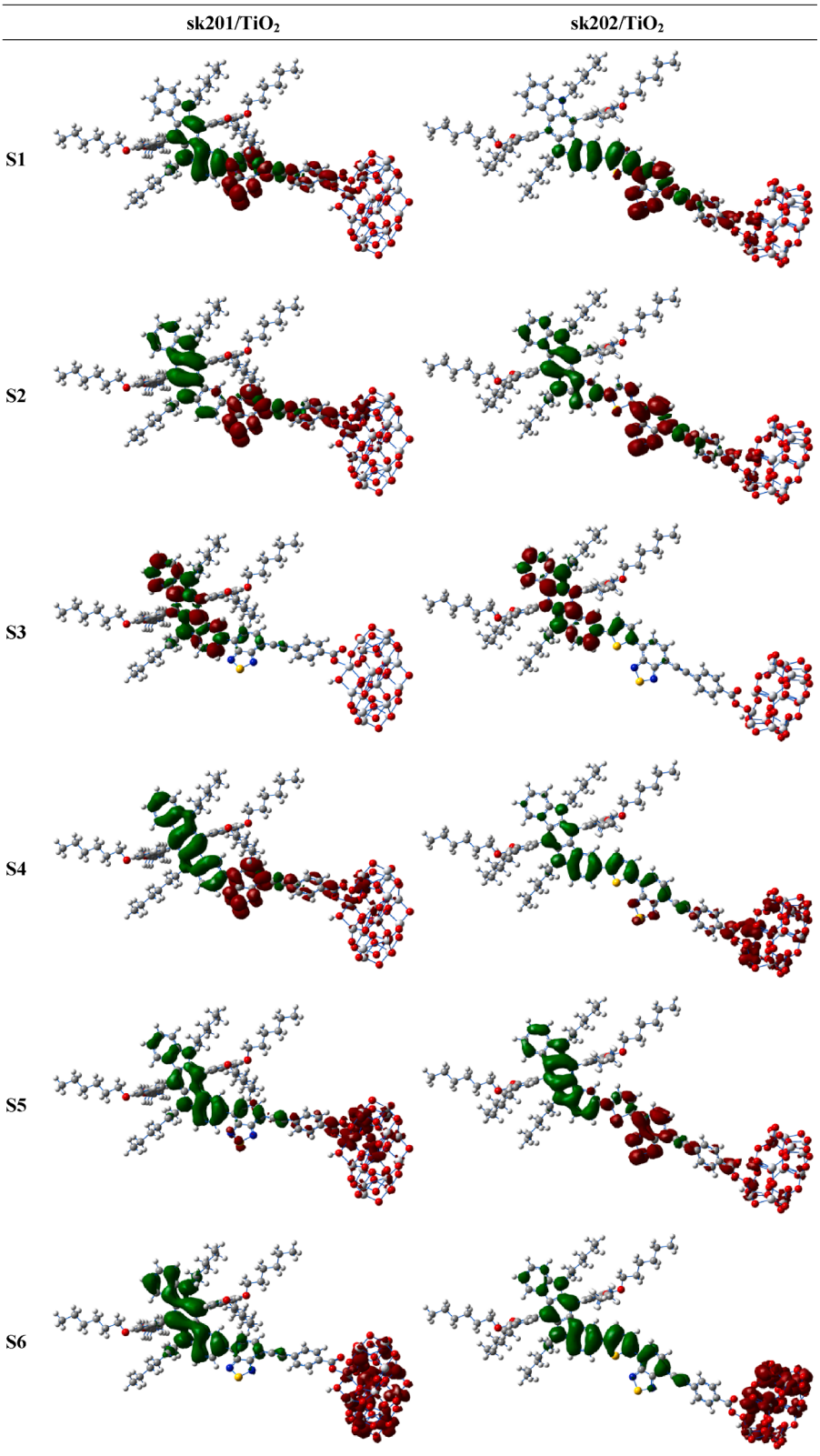

Fig. 5. Charge difference density of dye/TiO_2 complexes in DCM solvent.

Molecular electrostatic potential

The molecular electrostatic potential (ESP) produced by the nuclei and electrons in the space around a molecule, is an important method to predict and explain chemical reactions. In this work, ESP is used to reflect molecular electrophilic and nucleophilic reaction sites, which is crucial for investigating dye regeneration [42,43]. Different ESP values were described by different colors in Fig. 6, in which the blue (negative) areas and red (positive) areas correspond to the sites of nucleophilic and electrophilic reactions, respectively. The most positive sites of ESP

Table 2
Calculated hole reorganization energy (λ_h/eV), electron reorganization energy (λ_e/eV) and total reorganization energy (λ_{total}/eV) of dyes.

Dyes	λ_h	λ_e	λ_{total}
sk201	0.139	0.232	0.371
sk202	0.115	0.200	0.315

correspond to the most vital ability to attract electrons, that is, the most likely site to combine negative charges and electrolyte ions. As shown in Fig. 6, the red area of sk202 is significantly darker than sk201, which means that the dye regeneration ability of sk202 is stronger than sk201. Moreover, some cyan dots and orange dots on the ESP surface are the maximum and minimum points of ESP, respectively. Thus, the orange dots are the most likely sites that bind to electrolyte ions. For sk202, an orange dot happens to be at the sulfur atom thiophene, a likely site where the electrolyte ions may bind. From the above two aspects, the introduction of thiophene is beneficial to the regeneration of dyes. It is worth noting that iodide and triiodide are both anionic and could both bind to thiophene units, which would promote charge recombination of the photo-oxidize dyes [54]. However, more accumulation of triiodide near the surface of TiO_2 will result in increased interfacial recombination and further decreased value of Voc.

Nonlinear optical (NLO) properties

The dyes with excellent ICT capacity usually exhibit better NLO properties [55], described by the first hyperpolarizability (β_{tot}). β_{tot} that can be calculated via [56]:

$$\beta_{tot} = \left[\left(\beta_{xxx} + \beta_{xyy} + \beta_{xzz}\right)^2 + \left(\beta_{yyy} + \beta_{yzz} + \beta_{yxx}\right)^2 + \left(\beta_{zzz} + \beta_{zxx} + \beta_{zyy}\right)^2 \right] \quad (5)$$

where β_{ijk} ($i, j, k = x, y, z$) are the tensor components of the first hyperpolarizability. The obtained β_{ijk} and β_{tot} were listed in Table 3. sk202 has a bigger β_{tot}, which may be due to its smallest overall twist structure, indicating an ICT capacity. This conclusion is consistent with the previous analysis. Moreover, the value of β_{xxx} is much larger than the other components of β_{tot}, which means β_{tot} is dominated by β_{xxx}, and the electron transfer between the donors and acceptors is unidirectional.

Photoelectric parameters of DSSCs

For further investigating the photovoltaic performances of the dyes, key parameters were investigated quantificationally in this section. The overall PCE (η) is a crucial parameter for evaluating the photovoltaic performances of DSSCs. It is determined by J_{SC} (short-circuit photocurrent density), V_{OC} (open-circuit photovoltage), P_{inc} (incident light power) and *FF* (fill factor) from equation [5]:

$$\eta = FF\frac{J_{Sc} \cdot V_{OC}}{P_{inc}} \quad (6)$$

Therefore, η can be enhanced by increasing J_{SC} and V_{OC}.

J_{SC} is related to the efficiency of electron injection ϕ_{inj}, the charge collective efficiency (η_{coll}) and LHE through the following integral carried over the whole solar spectrum [5]:

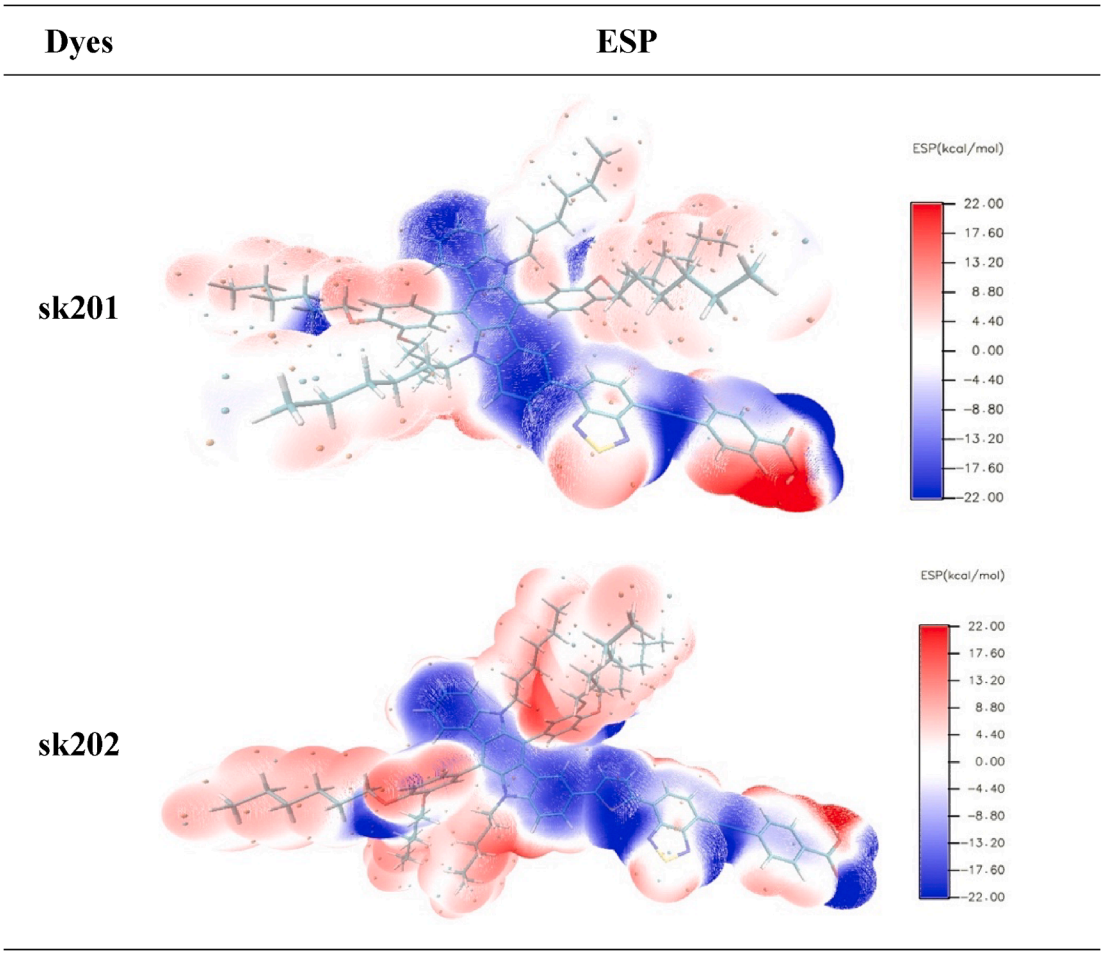

Fig. 6. ESP maps of sk201 and sk202 in DCM solvent.

Table 3
First hyperpolarizability (β_{tot}) and it's tensor components (β_{ijk}) of dyes (1×10^{-30} esu).

Dyes	β_{xxx}	β_{xxy}	β_{xyy}	β_{yyy}	β_{xxz}	β_{xyz}	β_{yyz}	β_{xzz}	β_{yzz}	β_{zzz}	β_{tot}
sk201	−736.94	−253.98	−97.16	−45.59	74.86	22.73	6.50	−9.64	−1.96	−0.34	899.66
sk202	1812.40	−545.86	161.23	−51.13	75.56	−20.72	4.94	2.73	−1.12	−0.25	2066.46

$$J_{Sc} = \int LHE(\lambda)\phi_{inj}\eta_{coll}d\lambda \tag{7}$$

For approximate calculations, η_{coll} is presumed to be uniform for all molecules in one dye. Based on Beer's law, *LHE* is a function of *f* and can be calculated by [57]:

$$LHE = 1 - 10^{-f} \tag{8}$$

ϕ_{inj} is related to the electron injection driving force (ΔG^{inject}) and electron regeneration driving force (ΔG^{regen}). ΔG^{inject} has the following expression [58]:

$$\Delta G^{inject} = E^{dye*} - E_{CB} = E^{dye} - E_{EX} - E_{CB} \tag{9}$$

where E^{dye*} and E^{dye} are the excited-state oxidation potential and the ground-state redox potential, respectively. E_{EX} is the excitation energy for the transition associated with the ICT. ΔG^{regen} can be used to characterize the regenerative capability of dyes from electrolyte, and can be calculated by [59]:

$$\Delta G^{regen} = E_{redox} - E^{dye} \tag{10}$$

On the other hand, V_{OC} is contributed by several factors, such as the E_{redox}, the E_{CB} and its shift (ΔE_{CB}) when adsorbing on the TiO_2, the densities of free electrons (n_c) and of accessible states (N_{CB}) in the CB of TiO_2, via the following expression [60]:

$$V_{OC} = \frac{E_{CB} + \Delta E_{CB}}{q} + \frac{kT}{q} ln\left(\frac{n_c}{N_{CB}}\right) - \frac{E_{redox}}{q} \tag{11}$$

ΔE_{CB} can be calculated by [61]:

$$\Delta E_{CB} = \frac{q\mu_{normal}\gamma}{\varepsilon_0 \varepsilon} \tag{12}$$

where q represents the unit charge, μ_{normal} denotes the vertical dipole moment of the dyes in the ground state, γ is the molecular surface concentration, ε_0 and ε denote the vacuum permittivity and dielectric permittivity, respectively.

The parameters mentioned above (E^{dye*}, ΔG^{regen}, ΔG^{inject}, μ_{normal} and *LHE*) of sk201 and sk202 were calculated and summarized in Table 4. For E^{dye*}, the smaller it is, the easier the dyes are to generate the photoexcitation, which is the first step for DSSC operation. From Table 4, sk201 has a smaller E^{dye*} (2.013 eV in gas and 2.165 eV in DCM solvent) than sk202 (2.234 eV in gas and 2.410 eV in DCM solvent), indicating that sk201 is more susceptible to photoexcitation. ΔG^{inject} is closely related to ϕ_{inj} in the way that a larger absolute value of ΔG^{inject} will be conducive to the electron injection and then improve the J_{SC}. From Table 4, sk201 has a larger absolute value of ΔG^{inject} than sk202. It was also reported that when the absolute value of ΔG^{inject} is greater than 0.2 eV, ϕ_{inj} can be considered to reach 1 [62]. From this point of view, both sk201 and sk202 can generate sufficiently effective electron injection, thus the electron injection efficiency will not be the main factor for the two primary dyes that cause the difference in J_{SC}. ΔG^{regen} is used to characterize the regenerative capability of dyes from electrolyte. A larger ΔG^{regen} will contribute to better dye reorganization ablility. From Table 4, ΔG^{regen} follows the order in both vacuum and solvent: sk201 > sk202, which means sk201 has better dye reorganization ablility. Besides, Eq. (7) shows that a bigger *LHE* will lead to a bigger J_{SC}. Table 4 shows that the *LHE*s are 0.869 and 0.956 in gas, 0.908 and 0.970 in DCM solvent for sk201 and sk202, respectively. Considering that sk202 is only superior to sk201 on LHE, and sk202 has a higher experimental J_{SC} [29], it can be concluded that the contribution of LHE plays a more important role in determining the J_{SC} for the investigated dyes. On the other hand, it was reported that V_{OC} was linearly dependent on the μ_{normal} of the ground-state dyes. From Table 4, sk202 has a bigger value of μ_{normal} than that of sk201 in both gas (sk201: 7.708, sk202: 10.310) and solvent (sk201: 7.747, sk202: 13.110), which causes the V_{OC} of sk202 to be greater than sk201. It can also be found that the solvent effect significantly increases the μ_{normal} of sk202 (gas: 10.310, DCM: 13.110) but has little impact on sk201 (gas: 7.708, DCM: 7.747). The above analysis on J_{SC} and V_{OC} explained the experimental results [29] from different angles. Besides, the lifetime (τ) in the dyes' excited state also has important effects on the charge transfer efficiency. It is determined by the excitation energy (E_g) and the corresponding (*f*) via:

$$\tau = \frac{1.499}{fE_g^2} \tag{13}$$

The calculated τs of sk201 and sk202 are 3.416 ns and 2.755 ns in gas, 2.932 ns and 2.555 ns in solvent, respectively.

Table 4
Calculated photoelectric parameters of sk201 and sk202.

	Dyes	E^{dye*}/eV	ΔG^{regen}	ΔG^{inject}/eV	LHE	μ_{normal}	τ/ns
Gas	sk201	2.013	0.175	−1.98	0.869	7.708	3.416
	sk202	2.234	0.117	−1.77	0.956	10.310	2.755
DCM	sk201	2.165	0.121	−1.83	0.908	7.747	2.932
	sk202	2.410	0.045	−1.60	0.970	13.110	2.555

Molecular design

Considering the important role of thiophene in leading to the excellent performance of sk202, three new dyes (DMZ1-3) were designed by further modifying thiophene with other units. The chemical structures of the designed dyes were shown in Fig. 7. All calculations in this section were only performed in DCM solvent. As previously discussed for sk201 and sk202, two selected dihedral angles were calculated and numerically shown in Fig. 7. From Fig. 7, DMZ1 shows the best overall planarity in all primary and designed dye molecules, which will theoretically make DMZ1 have the best ICT performance. Comparing sk202 and DMZ3, it is clear that the alkyl chain's introduction to thiophene makes DMZ3 exhibit a bigger twist structure than sk202.

The simulated absorption spectra curves of the designed dyes in the DCM solvent were shown in Fig. 8, which also exhibits the typical dual absorption peaks. The main absorption peaks located in the visible region are 527 nm, 476 nm and 481 nm for DMZ1, DMZ2 and DMZ3, respectively, caused by the transition of HOMO → LUMO. Moreover, it can be seen from Fig. 8 that both the width and molar absorption coefficient of the prominent absorption peaks follows the order: DMZ1 > DMZ3 > DMZ2. Comparing with sk202, DMZ1 shows an apparent redshift of 17.82 nm, while DMZ2 and DMZ3 have different degrees of blue shifts (33 nm and 28 nm). Besides, DMZ1 also has a higher molar absorption coefficient than sk202, whereas DMZ2 and DMZ3 show different degrees of decrease in the molar extinction coefficient. It is reasonable to believe that different planarity leads to different wavelengths of absorption peaks and different molar absorption coefficients for sk202 and DMZ1-3. Based on the above discussions, DMZ1 exhibits the best light-harvesting capacity in all investigated dyes due to its best molecular planarity.

To make a further quantitative comparison between the designed dyes and the primary dyes, the previously defined photoelectric pa-

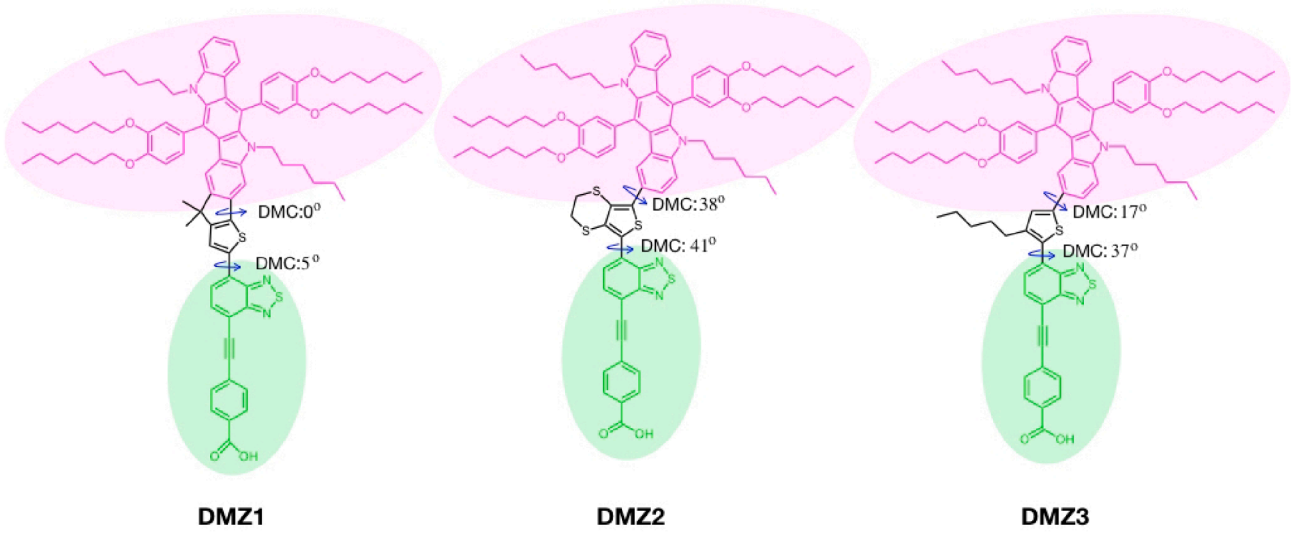

Fig. 7. Chemical structures of the designed dyes (DMZ1, DMZ2 and DMZ3).

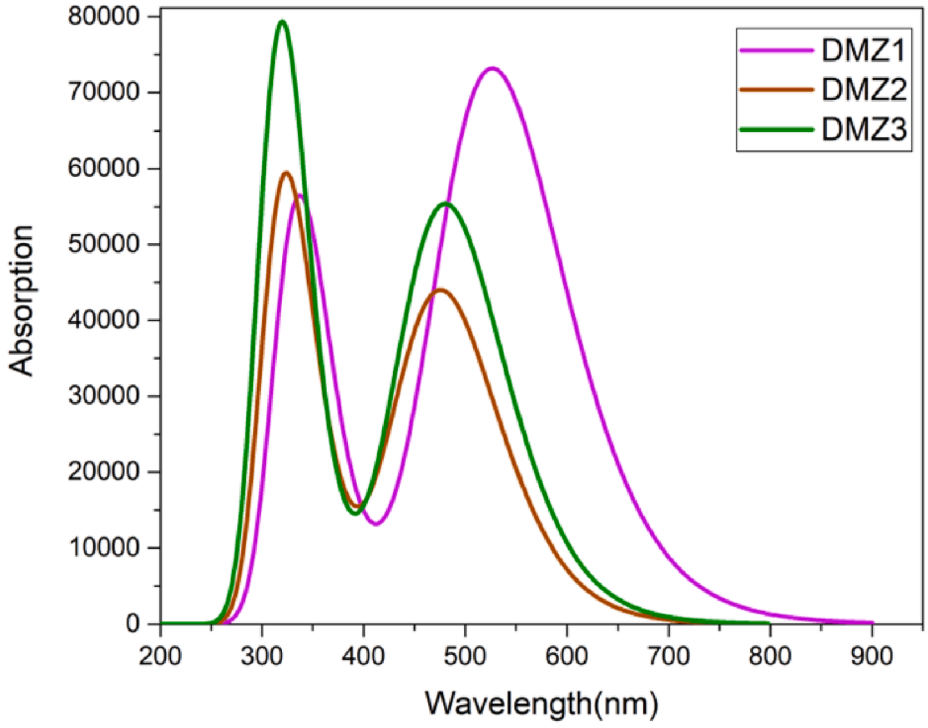

Fig. 8. Simulated absorption curves of (DMZ1, DMZ2 and DMZ3).

rameters (HOMO energy, LUMO energy and their gap, E^{dye*}, ΔG^{regen}, ΔG^{inject}, *LHE*, μ_{normal} and τ) were also calculated in DCM solvent for the designed dyes and were summarized in Table 5. From Table 5, the HOMOs of DMZ1-3 are −4.893 eV, −4.874 eV and −4.833 eV, respectively, which are all lower than −4.8 eV. The LUMOs of DMZ1-3 are −2.873 eV, −2.810 eV and −2.757 eV, respectively, which are all higher than −4.0 eV. Their gaps are 2.020 eV, 2.064 eV and 2.076 eV for DMZ1-3, respectively, which shows no noteworthy difference compared with sk202 (2.009 eV). The electron injection driving forces (ΔG^{inject}) are −1.46 eV, −1.73 eV and −1.75 eV for DMZ1-3, respectively, which are sufficient for the effective electron injection. As for ΔG^{regen}, the reorganization ablilities of dyes follow the order: DMZ1 > DMZ2 > DMZ3.

Table 5
Calculated photoelectric parameters of (DMZ1, DMZ2 and DMZ3).

Dyes	HOMO/eV	LUMO/eV	Gap/eV	E^{dye*}/eV	ΔG^{inject}/eV	ΔG^{inject}/eV	LHE	μ_{normal}	τ/ns
DMZ1	−4.893	−2.873	2.020	2.540	0.093	−1.46	0.984	9.096	2.31
DMZ2	−4.874	−2.810	2.064	2.270	0.074	−1.73	0.918	12.915	3.13
DMZ3	−4.833	−2.757	2.076	2.253	0.033	−1.75	0.957	13.501	2.53

Moreover, the *LHE* of DMZ1 is the largest in all investigated dyes and even larger than that of sk202. Specifically, the *LHE*s follow the order: DMZ1 (0.984) > sk202 (0.970) > DMZ 3 (0.957) > DMZ2 (0.918), which is consistent with the conclusions obtained based on the absorption spectra analysis. Considering the above analysis, it can be concluded that DMZ1 theoretically has a higher short-circuit current than sk202 and other designed dyes. For the vertical dipole moment (μ_{normal}), DMZ1-3 and two primary dyes follow the order: sk201(7.747) < DMZ1 (9.096) < DMZ2 (12.915) < sk202 (13.110) < DMZ3 (13.501). In theory, the open circuit voltage will also have the same order as the dipole moment. Based on the above analysis, it can be inferred that the introduction of the alkyl chain to thiophene leads to a decrease in LHE (sk202: 0.970, DMZ3: 0.957) while increasing the μ_{normal} (sk202: 13.110, DMZ3: 13.501). Besides, DMZ1, which is excellent in other aspects, may generate a low open-circuit voltage due to the smallest dipole moment.

Conclusions

Based on DFT and TD-DFT, two primary and three further designed dihydroindolocarbazole-based organic dyes (sk201, sk202 and DMZ1-3) were systemically investigated in the context of DSSCs. Their molecular geometries, electronic structures, absorption spectra, charge transfer, molecular ESP and NLO properties were studied to reveal the structure-properties relationships. Some key photoelectric parameters (including the oxidation potential, electron injection driving force, electron regeneration driving force, vertical dipole moment, light-harvesting efficiency, and excited-state lifetime), which are closely related to the PCEs of DSSCs, were calculated, and then analyzed by comparison. The conclusions obtained in this work can be summarized as follows: (1) By introducing a thiophene unit between the electron donor (DDC) and the electron acceptor (BTZ), sk202 shows relatively better overall planarity, stronger absorption of light in visible region, narrower gap between HOMO and LUMO, better ICT capability and larger first hyperpolarizability than sk201, indicating that sk202 is more conducive to improve the efficiency of DSSCs. (2) The effect of joining the isolated dye molecule (sk201 and sk202) and $(TiO_2)_9$ together on the properties of dye/TiO_2 complexes were investigated. For the two primary dyes, after absorbing on TiO_2, molar extinction coefficients are significantly increased, with only slight blue-shifts (sk201: 4 nm, sk202: 6 nm) in the maximum absorption wavelengths. Moreover, excellent ICT processes occur in both sk201/TiO_2 and sk202/TiO_2. (3) Calculations of some key photoelectric parameters show that sk202 exhibits advantages over sk201 in both LHE and μ_{normal}, which will lead to a greater PCE for sk202. (4) Three newly designed dyes (DMZ1-3) were investigated to further reveal the effect of modified thiophene on the performances of dyes. It is found that DMZ1 has the best overall planarity and strongest absorption spectrum, leading to the best LHE. Meanwhile, DMZ1 has the smallest μ_{normal}, indicating the smallest V_{OC}. For DMZ3, the introduction of alkyl chain to thiophene will cause a decrease in LHE and an increase in μ_{normal}.

CRediT authorship contribution statement

Qian Liu: Conceptualization, Methodology, Writing - review & editing, Funding acquisition. **Shihan Zhao:** Software, Formal analysis, Writing - original draft. **Yanhua Zhai:** Formal analysis, Investigation, Funding acquisition. **Ming Xu:** Validation, Funding acquisition. **Miao Li:** Visualization, Funding acquisition. **Xianbin Zhang:** Methodology, Supervision, Funding acquisition.

Declaration of Competing Interest

The authors declare that they have no known competing financial interests or personal relationships that could have appeared to influence the work reported in this paper.

Acknowledgements

This work was supported by the National Natural Science Foundation of China (grant numbers: 51877177, 61377036, 60971015); the Scientific Research Program Funded by Shaanxi Provincial Education Department (grant number: 19JC032); the Innovation Capability Support Plan of Shaanxi Province (grant number: 2018PT-27); the Natural Science Basic Research Plan of Shaanxi Province (grant number: 2019JQ-097); the Youth Innovation Team of Shaanxi Universities (Ultrafast Optoelectronic Devices and Materials Innovation Group); the State Key Laboratory of Infrared Physics, Chinese Academy of Sciences (grant number: M201919); and the National Scholarship Fund of China (No. 201808615021). Y. Z. was supported by the NSF EFMA-1741693, NSF 1806519, and Kennesaw State University. Q. L. is also grateful for the support from Kennesaw State University.

Appendix A. Supplementary data

Supplementary data to this article can be found online at https://doi.org/10.1016/j.rinp.2021.103939.

References

[1] Armaroli N, Balzani V. The future of energy supply: challenges and opportunities. Angew Chem Int Ed 2007;46(1-2):52–66. https://doi.org/10.1002/anie.200602373.
[2] Hoekstra AY, Wiedmann TO. Humanity's unsustainable environmental footprint. Science 2014;344(6188):1114–7. https://doi.org/10.1126/science:1248365.
[3] Pike R, Earis P. Powering the world with sunlight. Energy Environ Sci 2010;3:173. https://doi.org/10.1039/B924940K.
[4] O'Regan B, Grätzel M. A low-cost, high-efficiency solar cell based on dye-sensitized colloidal TiO_2 films. Nature 1991;353:737–40. https://doi.org/10.1038/353737a0.
[5] Hagfeldt A, Boschloo G, Sun L, Kloo L, Pettersson H. Dye-sensitized solar cells. Chem Rev 2010;110(11):6595–663. https://doi.org/10.1021/cr900356p.
[6] Roslan N, Ya'acob ME, Radzi MAM, Hashimoto Y, Jamaludin D, Chen G. Dye sensitized solar cell (DSSC) greenhouse shading: new insights for solar radiation manipulation. Renew Sustain Energy Rev 2018;92:171–86. https://doi.org/10.1016/j.rser.2018.04.095.
[7] Sharma K, Sharma V, Sharma SS. Dye-sensitized solar cells: fundamentals and current status. Nanoscale Res Lett 2018;13:381. https://doi.org/10.1186/s11671-018-2760-6.
[8] Nazeeruddin MK, Kay A, Rodicio I, Humphry-Baker R, Müller E, Liska P, et al. Conversion of light to electricity by cis-X_2Bis(2,2′-bipyridyl-4,4′- dicarboxylate) ruthenium(II) charge-transfer sensitizers ($X = Cl^-, Br^-, I^-, CN^-$) on nanocrystalline TiO_2 electrodes. J Am Chem Soc 1993;115:6382–90. https://doi.org/10.1021/ja00067a063.
[9] Wang P, Zakeeruddin SM, Moser JE, Nazeeruddin MK, Sekiguchi T, Grätzel M. A stable quasi-solid-state dye-sensitized solar cell with an amphiphilic ruthenium sensitizer and polymer gel electrolyte. Nat Mater 2003;2(6):402–7. https://doi.org/10.1038/nmat904.
[10] Han L, Islam A, Chen H, Malapaka C, Chiranjeevi B, Zhang S, et al. High-efficiency dye-sensitized solar cell with a novel co-adsorbent. Energy Environ Sci 2012;5(3):6057. https://doi.org/10.1039/c2ee03418b.
[11] Mathew S, Yella A, Gao P, Humphry-Baker R, Curchod BFE, Ashari-Astani N, et al. Dye-sensitized solar cells with 13% efficiency achieved through the molecular engineering of porphyrin sensitizers. Nat Chem 2014;6(3):242–7. https://doi.org/10.1038/nchem.1861.
[12] Kakiage K, Aoyama Y, Yano T, Oya K, Fujisawa J-I, Hanaya M. Highly-efficient dye-sensitized solar cells with collaborative sensitization by silyl-anchor and carboxy-anchor dyes. Chem Commun 2015;51(88):15894–7. https://doi.org/10.1039/C5CC06759F.
[13] Robertson N. Optimizing dyes for dye-sensitized solar cells. Angew Chem Int Ed 2006;45(15):2338–45. https://doi.org/10.1002/anie.200503083.
[14] Mishra A, Fischer MR, Bäuerle P. Metal-free organic dyes for dye-sensitized solar cells: from structure: property relationships to design rules. Angew Chem Int Ed 2009;48(14):2474–99. https://doi.org/10.1002/anie.200804709.
[15] Vougioukalakis GC, Philippopoulos AI, Stergiopoulos T, Falaras P. Contributions to the development of ruthenium-based sensitizers for dye-sensitized solar cells. Coord Chem Rev 2011;255(21-22):2602–21. https://doi.org/10.1016/j.ccr.2010.11.006.
[16] Yen YS, Chou HH, Chen YC, Hsu CY, Lin JT. Recent developments in molecule-based organic materials for dye-sensitized solar cells. J Mater Chem 2012;22:8734–47. https://doi.org/10.1039/C2JM30362K.
[17] Liang M, Chen J. Arylamine organic dyes for dye-sensitized solar cells. Chem Soc Rev 2013;42:3453–88. https://doi.org/10.1039/C3CS35372A.
[18] Lee C-P, Li C-T, Ho K-C. Use of organic materials in dye-sensitized solar cells. Mater Today 2017;20(5):267–83. https://doi.org/10.1016/j.mattod.2017.01.012.

[19] Kumavat PP, Sonar P, Dalal DS. An overview on basics of organic and dye sensitized solar cells, their mechanism and recent improvements. Renew Sustain Energy Rev 2017;78:1262–87. https://doi.org/10.1016/j.rser.2017.05.011.

[20] Iqbal MZ, Ali SR, Khan S. Progress in dye sensitized solar cell by incorporating natural photosensitizers. Sol Energy 2019;181:490–509. https://doi.org/10.1016/j.solener.2019.02.023.

[21] Sun K, Liu Y, Wu Y, Guo X, Li J, Wang L. Application of quantitative prediction to design new organic dyes in dye sensitized solar cells. J Mol Liq 2019;278:484–90. https://doi.org/10.1016/j.molliq.2019.01.078.

[22] Lu T-F, Li W, Zhang H-X. Rational design of metal-free organic D-π-A dyes in dye-sensitized solar cells: Insight from density functional theory (DFT) and time-dependent DFT (TD-DFT). Org Electron 2018;59:131–9. https://doi.org/10.1016/j.orgel.2018.05.005.

[23] Galappaththi K, Lim A, Ekanayake P, Petra MI. 3Cyanidin-based novel organic sensitizer for efficient dye-sensitized solar cells: DFT/TDDFT study. Int J Photoenergy 2017;2017:1–6. https://doi.org/10.1155/2017/8564293.

[24] Liu Y, Cao Y, Zhang W, Stojanovic M, Dar MI, Péchy P, et al. Electron-affinity-triggered variations on the optical and electrical properties of dye molecules enabling highly efficient dye-sensitized solar cells. Angew Chem Int Ed 2018;57(43):14125–8. https://doi.org/10.1002/anie.201808609.

[25] Ren Y, Sun D, Cao Y, Tsao HN, Yuan Yi, Zakeeruddin SM, et al. A stable blue photosensitizer for color palette of dye-sensitized solar cells reaching 12.6% efficiency. J Am Chem Soc 2018;140(7):2405–8. https://doi.org/10.1021/jacs.7b1234810.1021/jacs.7b12348.s001.

[26] Cheng Y, Yang G, Jiang H, Zhao S, Liu Q, Xie Y. Organic sensitizers with extended conjugation frameworks as cosensitizers of porphyrins for developing efficient dye-sensitized solar cells. ACS Appl Mater Interface 2018;10(45):38880–91. https://doi.org/10.1021/acsami.8b12883.s001.

[27] Zeng K, Lu Y, Tang W, Zhao S, Liu Q, Zhu W, et al. Efficient solar cells sensitized by a promising new type of porphyrin: dye-aggregation suppressed by double strapping. Chem Sci 2019;10(7):2186–92. https://doi.org/10.1039/C8SC04969F.

[28] Desta MB, Vinh NS, Kumar CP, Chaurasia S, Wu W-T, Lin JT, et al. Pyrazine-incorporating panchromatic sensitizers for dye sensitized solar cells under one sun and dim light. J Mater Chem A 2018;6:13778–89. https://doi.org/10.1039/C8TA04774J.

[29] Song X, Yang X, Wang H, An J, Yu Ze, Wang X, et al. Improving energy transfer efficiency of dye-sensitized solar cell by fine tuning of dye planarity. Sol Energy 2019;187:274–80. https://doi.org/10.1016/j.solener.2019.05.053.

[30] Parr RG. Density functional theory. Annu Rev Phys Chem 1983;34(1):631–56. https://doi.org/10.1146/annurev.pc.34.100183.003215.

[31] Jones RO. Density functional theory: Its origins, rise to prominence, and future. Rev Mod Phys 2015;87(3):897–923. https://doi.org/10.1103/RevModPhys.87.897.

[32] Furche F, Ahlrichs R. Adiabatic time-dependent density functional methods for excited state properties. J Chem Phys 2002;117(16):7433–47. https://doi.org/10.1063/1.1508368.

[33] Lee C, Yang W, Parr RG. Development of the Colle-Salvetti correlation-energy formula into a functional of the electron density. Phys Rev B 1988;37(2):785–9. https://doi.org/10.1103/PhysRevB.37.785.

[34] Becke AD. A new mixing of hartree-fock and local density-functional theories. J Chem Phys 1993;98(2):1372–7. https://doi.org/10.1063/1.464304.

[35] Hay PJ, Wadt WR. Ab initio effective core potentials for molecular calculations. Potentials for K to Au including the outermost core orbitals. J Chem Phys 1985;82(1):299–310. https://doi.org/10.1063/1.448975.

[36] Cossi M, Rega N, Scalmani G, Barone V. Structures, and electronic properties of molecules in solution with the C-PCM solvation model. J Comput Chem 2003;24:669–81. https://doi.org/10.1002/jcc.10189.

[37] Sánchez-de-Armas R, Oviedo López J, A. San-Miguel M, Sanz JF, Ordejón P, Pruneda M. Real-time TD-DFT simulations in dye sensitized solar cells: the electronic absorption spectrum of alizarin supported on TiO_2 nanoclusters. J Chem Theory Comput 2010;6(9):2856–65. https://doi.org/10.1021/ct100289t.

[38] Wu H, Ma T, Wu C, Yan L, Su Z. Effect of polyoxometalate in organic-inorganic hybrids on charge transfer and absorption spectra towards sensitizers. Dyes Pigments 2017;142:379–1368. https://doi.org/10.1016/j.dyepig.2017.03.062.

[39] Mu X, Wang J, Sun M. Visualizations of photoinduced charge transfer and electron-hole coherence in two-photon absorptions. J Phys Chem C 2019;123:14132. https://doi.org/10.1021/acs.jpcc.9b00700.

[40] Xu Z, Li Y, Zhang W, Yuan S, Hao L, Xu T, et al. DFT/TD-DFT study of novel T shaped phenothiazine-based organic dyes for dye-sensitized solar cells applications. Spectrochim Acta Part A 2019;212:272–80. https://doi.org/10.1016/j.saa.2019.01.002.

[41] Zhao D, Saputra RM, Song P, Yang Y, Li Y. How graphene strengthened molecular photoelectric performance of solar cells: a photo current-voltage assessment. Sol Energy 2021;213:271–83. https://doi.org/10.1016/j.solener.2020.11.034.

[42] Liu Q, Wang Q, Xu M, Liu J, Liang J. DFT characterization and design of anthracene-based molecules for improving spectra and charge transfer. Spectrochim Acta Part A 2020;227:117627. https://doi.org/10.1016/j.saa.2019.117627.

[43] Yanai T, Tew DP, Handy NC. A new hybrid exchange-correlation functional using the Coulom-battenuating method (CAM-B3LYP). Chem Phys Lett 2004;393(1-3):51–7. https://doi.org/10.1016/j.cplett.2004.06.011.

[44] Frisch MJ, Trucks GW, Schlegel HB, Scuseria GE, Robb MA, Cheeseman JR, et al. Gaussian 16, Revision C.01; Gaussian, Inc., Wallingford CT; 2016.

[45] Lu T, Chen F. Multiwfn: a multifunctional wavefunction analyzer. J Comput Chem 2012;33(5):580–92. https://doi.org/10.1002/jcc.v33.510.1002/jcc.22885.

[46] Feng S, Li QS, Niehaus TA, Li ZS. Effects of different electron donating groups on dye regeneration and aggregation in phenothiazine-based dye-sensitized solar cells. Org Electron 2017;42:234–43. https://doi.org/10.1016/j.orgel.2016.12.043.

[47] Liang M, Xu W, Cai F, Chen P, Peng B, Chen J, et al. New triphenylamine-based organic dyes for efficient dye-sensitized solar cells. J Phys Chem C 2007;111:4465–72. https://doi.org/10.1021/jp076992d.

[48] Kavan L, Grätzel M, Gilbert SE, Klemenz C, Scheel HJ. Electrochemical and photoelectrochemical investigation of single-crystal anatase. J Am Chem Soc 1996;118(28):6716–23. https://doi.org/10.1021/ja954172l.

[49] Smith AG, Shuford KL. Electronic effects on a D-π-A organic sensitizer upon heteroatom substitutions in the π-bridge. J Photochem Photobiol A 2017;332:580–5. https://doi.org/10.1016/j.jphotochem.2016.10.006.

[50] Marcus RA. Electron transfer reactions in chemistry. Theory and experiment. Rev Mod Phys 1993;65(3):599–610. https://doi.org/10.1103/RevModPhys.65.599.

[51] Hush NS. Adiabatic rate processes at electrodes. I. energy–charge relationships. J Chem Phys 1958;28(5):962–72. https://doi.org/10.1063/1.1744305.

[52] Deng W-Q, Goddard WA. Predictions of hole mobilities in oligoacene organic semiconductors from quantum mechanical calculations. J Phys Chem B 2004;108(25):8614–21. https://doi.org/10.1021/jp0495848.

[53] Wang X, Li Y, Song P, Ma F, Yang Y. Effect of graphene between photoanode and sensitizer on the intramolecular and intermolecular electron transfer process. Phys Chem Chem Phys 2020;22(11):6391–400. https://doi.org/10.1039/C9CP06543A.

[54] Clifford JN, Martínez-Ferrero E, Palomares E. Dye mediated charge recombination dynamics in nanocrystalline TiO2 dye sensitized solar cells. J Mater Chem 2012;22:12415–22. https://doi.org/10.1039/C2JM16107A.

[55] Wei J, Li Y, Song P, Yang Y, Ma F. Enhancement of one- and two-photon absorption and visualization of intramolecular charge transfer of pyrenyl-contained derivatives. Spectrochim Acta Part A 2021;245:118897. https://doi.org/10.1016/j.saa.2020.118897.

[56] Maroulis G. Static hyperpolarizability of the water dimer and the interaction hyperpolarizability of two water molecules. J Chem Phys 2000;113(5):1813–20. https://doi.org/10.1063/1.481985.

[57] Ardo S, Meyer GJ. Photodriven heterogeneous charge transfer with transition-metal compounds anchored to tio_2 semiconductor surfaces. Chem Soc Rev 2009;38(1):115–64. https://doi.org/10.1039/B804321N.

[58] Katoh R, Furube A, Yoshihara T, Hara K, Fujihashi G, Takano S, et al. Efficiencies of electron injection from excited N3 dye into nanocrystalline semiconductor (ZrO_2, TiO_2, ZnO, Nb_2O_5, SnO_2, In_2O_3) films. J Phys Chem B 2004;108(15):4818–22. https://doi.org/10.1021/jp031260g.

[59] Li M, Kou Li, Diao L, Zhang Q, Li Z, Wu Q, et al. Theoretical study of WS-9-based organic sensitizers for unusual vis/NIR absorption and highly efficient dye-sensitized solar cells. J Phys Chem C 2015;119(18):9782–90. https://doi.org/10.1021/acs.jpcc.5b03667.

[60] Marinado T, Nonomura K, Nissfolk J, Karlsson MK, Hagberg DP, Sun L, et al. Langmuir 2010; 26: 2592–2598. https://doi.org/10.1021/la902897z.

[61] Rühle S, Greenshtein M, Chen S-G, Merson A, Pizem H, Sukenik CS, et al. Molecular adjustment of the electronic properties of nanoporous electrodes in dye-sensitized solar cells. J Phys Chem B 2005;109(40):18907–13. https://doi.org/10.1021/jp0514123.

[62] Islam A, Sugihara H, Arakawa H. Molecular design of ruthenium(II) polypyridyl photosensitizers for efficient nanocrystalline TiO_2 solar cells. J Photochem Photobiol A 2003;158:131–8. https://doi.org/10.1016/S1010-6030(03)00027-3.